IEEE Access
Multidisciplinary | Rapid Review | Open Access Journal

Received 4 January 2024, accepted 3 February 2024, date of publication 13 February 2024, date of current version 21 February 2024.

Digital Object Identifier 10.1109/ACCESS.2024.3365702

RESEARCH ARTICLE

Base Station-Driven PAPR Reduction Method Utilizing Null Space for MIMO-OFDM Systems With Amplify-and-Forward Relaying

ASUKA KAKEHASHI, (Graduate Student Member, IEEE), TAKANORI HARA, (Member, IEEE), AND KENICHI HIGUCHI, (Senior Member, IEEE)
Graduate School of Science and Technology, Tokyo University of Science, Noda, Chiba 278-8510, Japan
Corresponding author: Kenichi Higuchi (higuchik@rs.tus.ac.jp)

ABSTRACT This paper proposes a peak-to-average power ratio (PAPR) reduction method that utilizes the null space in a multiple-input multiple-output (MIMO) channel for downlink MIMO-orthogonal frequency division multiplexing (OFDM) signals with multiple-antenna amplify-and-forward (AF)-type relaying. In order to achieve sufficient coverage enhancement using beamforming with multiple antennas and relaying, the PAPR not only at the base station (BS) but also at the relay station (RS) should be reduced to suppress the amount of input backoff (IBO) in the non-linear power amplifier. However, performing complex signal processing for PAPR reduction at the AF-type RS is impractical and leads to the concern that the channel capacity (throughput) will be reduced due to processing delay. In the proposed method, the BS alternately repeats the signal processing for generating the signal to reduce the PAPR at the BS and the signal to reduce the PAPR at the RS, where the RS does not require any signal processing for PAPR reduction. The generated PAPR reduction signals are projected onto the null space of the overall MIMO channel of the entire system for each frequency block. Computer simulation results using the non-linear power amplifier model show that the proposed method achieves higher throughput compared to the clipping and filtering (CF) method for the BS by reducing the PAPR at the RS utilizing the null space of the channel.

INDEX TERMS Amplify-and-forward, multiple-input multiple-output (MIMO), null space, orthogonal frequency division multiplexing (OFDM), peak-to-average power ratio (PAPR), relaying, non-linear power amplifier, frequency-selective fading channel.

I. INTRODUCTION

The combination of massive multiple-input multiple-output (MIMO) [1], [2] using beamforming (BF) and orthogonal frequency division multiplexing (OFDM) signals offers wide-coverage enhanced mobile broadband. Furthermore, in the 5th generation mobile communication system (5G) New Radio (NR) [3] and beyond [4], the importance of relay transmission [5], [6], [7] increases in actualizing wide coverage in a high frequency band such as the millimeter-wave band. In this paper, we consider downlink MIMO-OFDM transmission using amplify-and-forward (AF)-type relaying. Here, the AF relay station (RS) is equipped with multiple antennas and transfers the received signal from the base station (BS) to a set of user equipment (UE) after power amplification without decoding the data signal.

The high peak-to-average power ratio (PAPR) of OFDM signals is a significant drawback. When a signal with a high PAPR is amplified by a power amplifier (PA), the amount of input backoff (IBO) must be increased in order to suppress the in-band and out-of-band distortion to allowable levels. This leads to a decrease in the transmission power. In massive MIMO, in which a PA is prepared for each of a large number of transmitter antennas, reducing the PAPR is particularly important. This problem is the same for the RS, and PAPR reduction for both the BS and RS transmitters is important

The associate editor coordinating the review of this manuscript and approving it for publication was Jad Nasreddine.

to achieve high-speed high-quality transmission with wide coverage through relaying.

In single-input single-output (SISO) or single-input multiple-output (SIMO) relay transmission, the problem of PAPR reduction for the RS is not so critical if the PAPR at the BS transmitter is reduced. However, in multiple-input single-output (MISO) or MIMO relay transmission, the problem of PAPR reduction for the RS is very important. The received signal at the RS is a superposition of many transmission signals from the BS. Even if the PAPR at the BS is reduced, the PAPR at the RS will increase again (see Fig. 3). Therefore, in MIMO relay transmission, PAPR reduction is very important not only for the BS but also for the RS in order to achieve sufficient coverage enhancement through relaying.

A. RELATED WORK

A number of PAPR reduction methods employing MIMO-OFDM have been investigated, *e.g.*, in [8], [9], [10], [11], [12], [13], [14], [15], and [16]. Among these methods, when a powerful channel code such as the turbo code or low-density parity check (LDPC) code is employed, [17] revealed that a PAPR reduction method that does not reduce the frequency efficiency at the cost of in-band interference such as the clipping and filtering (CF) method [9], [10] is superior to those that consume a part of the frequency bandwidth to reduce the PAPR such as the tone reservation method [13] from the viewpoint of the tradeoff between the PAPR reduction and the error rate. However, the in-band PAPR reduction signal added to the data signal at the transmitter by the CF method becomes a source of interference to the data streams at the receiver.

To address this problem, PAPR reduction methods utilizing a number of antennas at the BS that is sufficiently larger than the number of antennas at the UE receiver in a downlink massive MIMO environment were reported in [18], [19], [20], [21], [22], [23], [24], [25], and [26]. In [18] and [19], some of the antennas at the BS are used exclusively to transmit compensation signals that eliminate the PAPR reduction signal. The PAPR reduction signal transmitted from the antenna transmitting the data signal is canceled on the user terminal receiver end by the signal transmitted from the antenna exclusively transmitting the compensation signals, thereby avoiding interference caused by PAPR reduction. On the other hand, in [20], [21], [22], [23], [24], [25], and [26], PAPR reduction is performed by utilizing the null space of the downlink MIMO channel, which exists when the number of transmission antennas at the BS is larger than the number of receiver antennas at the UEs. This method restricts the PAPR reduction signal to be transmitted only to the null space in MIMO channels by using BF. This restriction suppresses interference to the data stream at the UE receiver due to PAPR reduction. Unlike the methods in [18] and [19], the method in [20], [21], [22], [23], [24], [25], and [26] can use all the transmitter antennas for data transmission and obtain a higher MIMO transmission gain (signal power gain and interference suppression gain due to BF).

There have been various studies on PAPR reduction methods for OFDM signals in AF-relay transmission when the BS has a single antenna. In [27], PAPR reduction based on CF is investigated. When applying oversampling, CF operations in the source node and/or relay nodes confirmed that the best results are achieved when the clipping process is applied at the source node. In [28], PAPR reduction based on a partial transmit sequence (PTS) is investigated. This study showed that the PTS scheme improves energy efficiency and spectral efficiency performance compared to no PAPR reduction in the OFDM relay system. In [29], a PAPR reduction method based on the superposition of the Golay sequence and the Reed-Muller code on the transmission signal is investigated. This study showed that the performance of this scheme for the source and relay nodes is much better than that for only the source node or the relay node. In [30], PAPR reduction in the RS based on best-to-worst (BTW) subcarrier pairing (SCP) is investigated. In this method, after BTW reordering, the PAPR is calculated and its value is compared with a threshold value. If the PAPR cannot achieve the required PAPR value, the subcarrier is one-by-one circularly shifted until it reaches the maximum number of shifts. If the PAPR is higher than the threshold even after reaching the maximum number of shifts, the signals are then clipped into the threshold value.

On the other hand, to the best of our knowledge, there have been only a few studies on PAPR reduction methods for OFDM signals in AF relay transmission when the BS has multiple antennas. Members of our research group reported a PAPR reduction method utilizing the null space in a MIMO channel for a multi-antenna AF-type RS [31], [32]. In this method, PAPR reduction utilizing the null space in the overall MIMO channel, which combines the channel between the BS and RS and that between the RS and the UEs, is applied to the transmission signal at the BS in advance. Then, the peak signal component observed again at the RS receiver due to the effect of the MIMO channel is reduced by generating a PAPR reduction signal at the RS that is transmitted only to the null space in the MIMO channel between the RS and UEs. This method enables PAPR reduction on both the BS and RS transmitter ends while suppressing the interference to the data stream at the UE receivers. However, this method requires complex signal processing at the RS for PAPR reduction. If there is a delay of at least 1 OFDM symbol duration caused by the signal processing for PAPR reduction at the RS, relay transmission using the same channel as that used at the BS, which is an advantage of AF relay transmission, will not be possible. Therefore, there is concern that a method that needs signal processing for PAPR reduction at the RS such as in [31] and [32] may incur a reduction in the channel capacity (throughput).

B. CONTRIBUTIONS AND ORGANIZATIONS

To address the problem in which signal processing is required for PAPR reduction at the RS, this paper proposes a method to achieve PAPR reduction for the RS transmitter using signal

processing at the BS while utilizing the null space in the MIMO channel. In this method, signal processing at the BS alternately and repeatedly generates PAPR reduction signals for the BS and RS transmitter ends. These PAPR reduction signals are projected onto the null space of the overall MIMO channel of the entire system. After iterative processing, these PAPR reduction signals are transmitted together from the BS. In conventional studies, it is not practical to perform PAPR reduction at the RS due to concerns regarding throughput degradation. However, the proposed method reduces the PAPR at the RS without PAPR reduction signal processing at the RS. Therefore, the proposed method reduces not only the PAPR at the BS but also the PAPR at the RS and achieves higher throughput by avoiding the throughput degradation caused by the delay due to PAPR reduction signal processing at the RS.

In this paper, we assume that the RS cannot perform PAPR reduction. Therefore, we define the conventional method as the application of CF for the BS [27] to AF relay transmission when the BS has multiple antennas and compare it to the proposed method. Computer simulations show that the proposed method achieves higher throughput compared to the methods that reduce only the PAPR at the BS such as CF for the BS. We also note that the preliminarily version of the proposed method was presented in [33] and this paper presents a concrete version of the proposed method and enhanced evaluation results.

The remainder of the paper is organized as follows. First, Section II describes the system model. Section III presents the proposed method. Section IV presents numerical results based on computer simulations. Finally, Section V concludes the paper.

II. SYSTEM MODEL

Fig. 1 shows the system model assumed in this paper. The distance between the BS and RS, that between the RS and UEs, and that between the BS and UEs are denoted as D_{BR}, D_{RU}, and D_{BU}, respectively. The number of BS antennas is N_{B} and that for RS antennas is N_{R}. We consider a downlink multiuser MIMO scenario where N_{U} users each having a single receiver antenna are spatially multiplexed. Assuming a massive MIMO environment, we set $N_{\mathrm{B}} \geq N_{\mathrm{R}} > N_{\mathrm{U}}$. The total number of subcarriers in the OFDM signals is K. There are B frequency blocks with different channel conditions from each other. The number of subcarriers in each frequency block is K/B. At frequency block b ($b = 1, .., B$), the $N_{\mathrm{R}} \times N_{\mathrm{B}}$-dimensional channel matrix between the BS and RS is denoted as $\mathbf{H}_{\mathrm{BR},b}$ and the $N_{\mathrm{U}} \times N_{\mathrm{R}}$-dimensional channel matrix between the RS and UEs is denoted as $\mathbf{H}_{\mathrm{RU},b}$. The $N_{\mathrm{U}} \times N_{\mathrm{B}}$-dimensional channel matrix of the direct link between the BS and UEs is denoted as $\mathbf{H}_{\mathrm{BU},b}$. The $N_{\mathrm{U}} \times N_{\mathrm{B}}$-dimensional channel matrix of the overall relay link is denoted as $\mathbf{H}_{\mathrm{BRU},b} = A_{\mathrm{R}}\mathbf{H}_{\mathrm{RU},b}\mathbf{H}_{\mathrm{BR},b}$ where A_{R} is a gain showing the power amplification operation in the RS including the IBO. The overall MIMO channel that combines the channels of the direct and relay links is denoted as $\mathbf{H}_{\mathrm{T},b} = \mathbf{H}_{\mathrm{BRU},b} + \mathbf{H}_{\mathrm{BU},b}$. It is assumed that the BS knows all channel matrixes in advance.

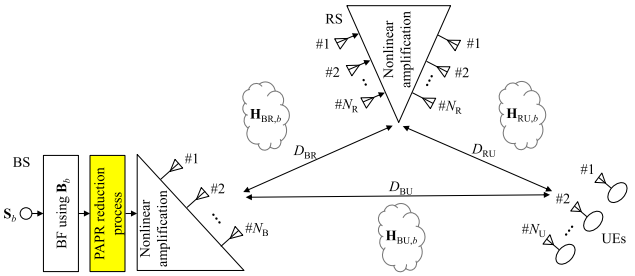

FIGURE 1. System model.

The N_{U}-dimensional data stream vector before BF on subcarrier k ($k = 1, \ldots, K/B$) of each frequency block b is denoted as $\mathbf{s}_{b,k}$. The BS generates the N_{B}-dimensional transmission signal vector after BF, $\mathbf{x}_{b,k}$, by multiplying $\mathbf{s}_{b,k}$ by $N_{\mathrm{B}} \times N_{\mathrm{U}}$-dimensional BF matrix $\mathbf{B}_b$. The proposed method presented in Section III can be applied to any BF method for data signals. In this paper, $\mathbf{B}_b$ is generated based on zero forcing (ZF) for overall channel matrix $\mathbf{H}_{\mathrm{T},b}$. Thus, $\mathbf{x}_{b,k}$ is represented as

$$\begin{aligned}\mathbf{x}_{b,k} &= \mathbf{B}_b\mathbf{s}_{b,k} = \mathbf{H}_{\mathrm{T},b}^{-}\mathbf{s}_{b,k} = (\mathbf{H}_{\mathrm{BRU},b} + \mathbf{H}_{\mathrm{BU},b})^{-}\mathbf{s}_{b,k} \\ &= (A_{\mathrm{R}}\mathbf{H}_{\mathrm{RU},b}\mathbf{H}_{\mathrm{BR},b} + \mathbf{H}_{\mathrm{BU},b})^{-}\mathbf{s}_{b,k} \end{aligned} \tag{1}$$

where $\mathbf{H}_{\mathrm{T},b}^{-}$ is a Moore-Penrose generalized inverse matrix of $\mathbf{H}_{\mathrm{T},b}$ ($\mathbf{H}_{\mathrm{T},b}^{-} = \mathbf{H}_{\mathrm{T},b}^{H}(\mathbf{H}_{\mathrm{T},b}\mathbf{H}_{\mathrm{T},b}^{H})^{-1}$).

The $N_{\mathrm{U}} \times K/B$-dimensional data stream matrix in frequency block b is denoted as $\mathbf{S}_b = [\,\mathbf{s}_{b,1} \cdots \mathbf{s}_{b,K/B}\,]$. The $N_{\mathrm{B}} \times K/B$-dimensional transmission data signal matrix, $\mathbf{X}_b$, in frequency block b is expressed by the following equation.

$$\begin{aligned}\mathbf{X}_b &= \mathbf{B}_b\mathbf{S}_b = \mathbf{H}_{\mathrm{T},b}^{-}\mathbf{S}_b = (\mathbf{H}_{\mathrm{BRU},b} + \mathbf{H}_{\mathrm{BU},b})^{-}\mathbf{S}_b \\ &= (A_{\mathrm{R}}\mathbf{H}_{\mathrm{RU},b}\mathbf{H}_{\mathrm{BR},b} + \mathbf{H}_{\mathrm{BU},b})^{-}\mathbf{S}_b. \end{aligned} \tag{2}$$

The transmission signal matrix at the BS after the PAPR reduction process is expressed as $\mathbf{X}_b + \mathbf{E}_b$, where $\mathbf{E}_b$ is the PAPR reduction signal matrix generated at the BS. $\mathbf{X}_b + \mathbf{E}_b$ is amplified by non-linear PAs and the in-band output signal, $\mathbf{X}_{\mathrm{B},b}$, at the BS can be written as

$$\mathbf{X}_{B,b} = A_{\mathrm{B}}(\mathbf{X}_b + \mathbf{E}_b) + \mathbf{D}_{\mathrm{B},b} \tag{3}$$

where A_{B} is a gain showing the power amplification operation in the BS including the IBO and $\mathbf{D}_{\mathrm{B},b}$ is the in-band non-linear distortion noise matrix by PAs at the BS in frequency block b.

The $N_{\mathrm{R}} \times K/B$-dimensional received signal matrix at the RS, $\mathbf{Y}_{\mathrm{R},b}$, is represented as

$$\mathbf{Y}_{\mathrm{R},b} = \mathbf{H}_{\mathrm{BR},b}\mathbf{X}_{\mathrm{B},b} + \mathbf{Z}_{\mathrm{R},b} \tag{4}$$

where $\mathbf{Z}_{\mathrm{R},b}$ is the noise matrix observed at the RS receiver in frequency block b. $\mathbf{Y}_{\mathrm{R},b}$ is amplified by non-linear PAs, and the in-band output signal, $\mathbf{X}_{\mathrm{R},b}$, at the RS can be written as

$$\mathbf{X}_{\mathrm{R},b} = A_{\mathrm{R}}\mathbf{Y}_{\mathrm{R},b} + \mathbf{D}_{\mathrm{R},b} \tag{5}$$

where $\mathbf{D}_{\mathrm{R},b}$ is the in-band non-linear distortion noise matrix by PAs at the RS in frequency block b.

The $N_{\mathrm{U}} \times K/F$-dimensional received signal matrix, $\mathbf{Y}_{\mathrm{U},b}$, at N_{U} UEs is expressed as the following.

$$\begin{aligned}\mathbf{Y}_{\mathrm{U},b} &= \mathbf{H}_{\mathrm{RU},b}\mathbf{X}_{\mathrm{R},b} + \mathbf{H}_{\mathrm{BU},b}\mathbf{X}_{\mathrm{B},b} + \mathbf{Z}_{\mathrm{U},b} \\ &= \mathbf{H}_{\mathrm{T},b}\mathbf{X}_{\mathrm{B},b} + \mathbf{H}_{\mathrm{RU},b}\mathbf{D}_{\mathrm{R},b} + A_{\mathrm{R}}\mathbf{H}_{\mathrm{RU},b}\mathbf{Z}_{\mathrm{R},b} + \mathbf{Z}_{\mathrm{U},b} \\ &= A_{\mathrm{B}}\mathbf{H}_{\mathrm{T},b}(\mathbf{X}_b + \mathbf{E}_b) + \mathbf{H}_{\mathrm{T},b}\mathbf{D}_{\mathrm{B},b} \\ &\quad + \mathbf{H}_{\mathrm{RU},b}\mathbf{D}_{\mathrm{R},b} + A_{\mathrm{R}}\mathbf{H}_{\mathrm{RU},b}\mathbf{Z}_{\mathrm{R},b} + \mathbf{Z}_{\mathrm{U},b} \\ &= A_{\mathrm{B}}\mathbf{S}_b + A_{\mathrm{B}}\mathbf{H}_{\mathrm{T},b}\mathbf{E}_b + \mathbf{H}_{\mathrm{T},b}\mathbf{D}_{\mathrm{B},b} \\ &\quad + \mathbf{H}_{\mathrm{RU},b}\mathbf{D}_{\mathrm{R},b} + A_{\mathrm{R}}\mathbf{H}_{\mathrm{RU},b}\mathbf{Z}_{\mathrm{R},b} + \mathbf{Z}_{\mathrm{U},b} \end{aligned} \tag{6}$$

where $\mathbf{Z}_{\mathrm{U},b}$ is the noise matrix observed at the UE receivers in frequency block b.

The objective of the proposed method is to achieve the required PAPR reduction not only at the BS but also at the RS while suppressing interference component $A_{\mathrm{B}}\mathbf{H}_{\mathrm{T},b}\mathbf{E}_b$ due to the PAPR reduction signal.

III. PROPOSED METHOD

In the proposed method, PAPR reduction signal processing is performed at the BS in the system model shown in Fig. 1. Specifically, the adaptive PAPR reduction method that uses the null space of the overall channel including direct and relay links, which is different for each frequency block, generates PAPR reduction signal matrix $\mathbf{E}_b$ that reduces the PAPR at the BS and RS while suppressing the interference to the data stream at the UE receivers. As an implementation algorithm of the PAPR reduction method utilizing the null space in the MIMO channel, two algorithms are considered in literature: CF followed by the channel-null constraint (CFCNC) [20], [21], [22] and peak cancellation (PC) signal with the channel-null constraint (PCCNC) [23], [24], [25], [26]. In this paper, the method based on CFCNC is examined to facilitate the analysis of the causes of differences from the conventional method, CF [27].

The proposed method alternately repeats generating the signal that reduces the PAPR at the BS transmitter and the signal that reduces the PAPR at the RS transmitter as shown in Fig. 2. The PAPR reduction signal matrix in frequency block b that reduces the PAPR at the RS transmitter generated at the j-th ($j = 1, \ldots, J$: J is the number of iterations) iteration is denoted as $\mathbf{E}^{(j)}_{\mathrm{R},b}$. Similarly, the PAPR reduction signal matrix in frequency block b that reduces the PAPR at the BS transmitter generated at the j-th iteration is denoted as $\mathbf{E}^{(j)}_{\mathrm{B},b}$. As the initial setting, $\mathbf{E}^{(0)}_{\mathrm{R},b}$ and $\mathbf{E}^{(0)}_{\mathrm{B},b}$ are set to zero.

In the following, we explain the proposed method focusing on signal processing in frequency block b. In the proposed method, the same processing is performed for all frequency blocks. At the j-th iteration, $\mathbf{E}^{(j)}_{\mathrm{R},b}$ is generated first. For the temporally assumed transmission signal matrix at the j-th iteration, $\mathbf{X}_b + \mathbf{E}^{(j-1)}_{\mathrm{R},b} + \mathbf{E}^{(j-1)}_{\mathrm{B},b}$, at the BS, received signal matrix $\tilde{\mathbf{Y}}^{(j)}_{\mathrm{R},b}$ at the RS is estimated as

$$\tilde{\mathbf{Y}}^{(j)}_{\mathrm{R},b} = \mathbf{H}_{\mathrm{B},b}(\mathbf{X}_b + \mathbf{E}^{(j-1)}_{\mathrm{R},b} + \mathbf{E}^{(j-1)}_{\mathrm{B},b}). \tag{7}$$

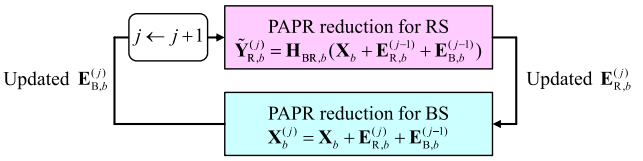

FIGURE 2. Iterative PAPR reduction process in the proposed method.

The K-dimensional time domain received signal vector, $\tilde{\mathbf{y}}^{(j)}_{\mathrm{R},n}$, at antenna n ($n = 1,\ldots, N_{\mathrm{R}}$) of the RS is expressed as

$$\begin{bmatrix} \tilde{\mathbf{y}}^{(j)}_{\mathrm{R},1} & \cdots & \tilde{\mathbf{y}}^{(j)}_{\mathrm{R},N_{\mathrm{R}}} \end{bmatrix} = \mathbf{F}^H \begin{bmatrix} \tilde{\mathbf{Y}}^{(j)}_{\mathrm{R},1} & \cdots & \tilde{\mathbf{Y}}^{(j)}_{\mathrm{R},B} \end{bmatrix}^T. \tag{8}$$

Here, $\mathbf{F}$ is the $K \times K$-dimensional fast Fourier transform (FFT) matrix and $\mathbf{F}^H$ is the inverse fast Fourier transform (IFFT) matrix. The time-domain PAPR reduction signal vector, $\tilde{\boldsymbol{\delta}}^{(j)}_{\mathrm{R},n}$, at antenna n of the RS is obtained by applying CF to $\tilde{\mathbf{y}}^{(j)}_{\mathrm{R},n}$ in order to reduce the PAPR. The $N_{\mathrm{R}} \times K/B$-dimensional frequency-domain PAPR reduction signal matrix in frequency block b is expressed as

$$\begin{bmatrix} \tilde{\mathbf{E}}^{(j)}_{\mathrm{R},1} & \cdots & \tilde{\mathbf{E}}^{(j)}_{\mathrm{R},B} \end{bmatrix} = \begin{bmatrix} \tilde{\boldsymbol{\delta}}^{(j)}_{\mathrm{R},1} & \cdots & \tilde{\boldsymbol{\delta}}^{(j)}_{\mathrm{R},N_{\mathrm{R}}} \end{bmatrix}^T \mathbf{F}^T. \tag{9}$$

In the proposed method, the PAPR reduction signal is transmitted from the BS. The PAPR reduction signal matrix to be transmitted from the BS, which is received as signal $\tilde{\mathbf{E}}^{(j)}_{\mathrm{R},b}$ at the RS, is expressed as $\mathbf{H}^{-}_{\mathrm{BR},b}\tilde{\mathbf{E}}^{(j)}_{\mathrm{R},b}$ where $\mathbf{H}^{-}_{\mathrm{BR},b}$ is the Moore-Penrose generalized inverse matrix of $\mathbf{H}_{\mathrm{BR},b}$. However, $\mathbf{H}^{-}_{\mathrm{BR},b}\tilde{\mathbf{E}}^{(j)}_{\mathrm{R},b}$ contains components that interfere with the data stream at the UE receivers. To remove the interference observed at the UE receivers, $\mathbf{H}^{-}_{\mathrm{BR},b}\tilde{\mathbf{E}}^{(j)}_{\mathrm{R},b}$ is projected onto the null space in overall MIMO channel $\mathbf{H}_{\mathrm{T},b}$. Since $\mathbf{H}_{\mathrm{T},b}$ is the $N_{\mathrm{U}} \times N_{\mathrm{B}}$-dimensional matrix and we assume $N_{\mathrm{B}} > N_{\mathrm{U}}$, we have $N_{\mathrm{B}} \times (N_{\mathrm{B}} - N_{\mathrm{U}})$-dimensional matrix $\mathbf{V}_{\mathrm{T},b}$ corresponding to the null space in $\mathbf{H}_{\mathrm{T},b}$. Thus, $\mathbf{H}_{\mathrm{T},b}\mathbf{V}_{\mathrm{T},b} = \mathbf{O}$ and we assume that all column vectors of $\mathbf{V}_{\mathrm{T},b}$ are orthonormal. By adding the projection of $\mathbf{H}^{-}_{\mathrm{BR},b}\tilde{\mathbf{E}}^{(j)}_{\mathrm{R},b}$ on $\mathbf{V}_{\mathrm{T},b}$ to $\mathbf{E}^{(j-1)}_{\mathrm{R},b}$, $\mathbf{E}^{(j-1)}_{\mathrm{R},b}$ is updated to $\mathbf{E}^{(j)}_{\mathrm{R},b}$ as

$$\mathbf{E}^{(j)}_{\mathrm{R},b} = \mathbf{E}^{(j-1)}_{\mathrm{R},b} + \mathbf{V}_{\mathrm{T},b}\mathbf{V}^H_{\mathrm{T},b}\mathbf{H}^{-}_{BR,b}\tilde{\mathbf{E}}^{(j)}_{\mathrm{R},b}. \tag{10}$$

Next, $\mathbf{E}^{(j)}_{B,b}$ is generated. PAPR reduction utilizing null space $\mathbf{V}_{\mathrm{T},b}$ in $\mathbf{H}_{\mathrm{T},b}$ is performed on the temporally assumed transmission signal matrix, $\mathbf{X}^{(j)}_b = \mathbf{X}_b + \mathbf{E}^{(j)}_{\mathrm{R},b} + \mathbf{E}^{(j-1)}_{\mathrm{B},b}$, at the BS. The K-dimensional time domain transmission signal vector, $\mathbf{y}^{(j)}_{\mathrm{B},n}$, at antenna n is expressed as

$$\begin{bmatrix} \mathbf{y}^{(j)}_{\mathrm{B},1} & \cdots & \mathbf{y}^{(j)}_{\mathrm{B},N_{\mathrm{B}}} \end{bmatrix} = \mathbf{F}^H \begin{bmatrix} \mathbf{X}^{(j)}_1 & \cdots & \mathbf{X}^{(j)}_B \end{bmatrix}^T. \tag{11}$$

The time-domain PAPR reduction signal vector, $\tilde{\boldsymbol{\delta}}^{(j)}_{\mathrm{B},n}$, at antenna n of the BS is obtained by applying CF to $\mathbf{y}^{(j)}_{\mathrm{B},n}$ in order to reduce the PAPR. The $N_{\mathrm{B}} \times K/B$-dimensional frequency domain PAPR reduction signal matrix, $\tilde{\mathbf{E}}^{(j)}_{\mathrm{B},b}$, in frequency block b is expressed as

$$\begin{bmatrix} \tilde{\mathbf{E}}^{(j)}_{\mathrm{B},1} & \cdots & \tilde{\mathbf{E}}^{(j)}_{\mathrm{B},B} \end{bmatrix} = \begin{bmatrix} \boldsymbol{\delta}^{(j)}_{\mathrm{B},1} & \cdots & \boldsymbol{\delta}^{(j)}_{\mathrm{B},N_{\mathrm{B}}} \end{bmatrix}^T \mathbf{F}^T. \tag{12}$$

To remove the interference observed at the UE receivers, $\tilde{\mathbf{E}}_{\mathrm{B},b}^{(j)}$ is projected onto $\mathbf{V}_{\mathrm{T},b}$ in $\mathbf{H}_{\mathrm{T},b}$. By adding the projection of $\tilde{\mathbf{E}}_{\mathrm{B},b}^{(j)}$ on $\mathbf{V}_{\mathrm{T},b}$ to $\mathbf{E}_{\mathrm{B},b}^{(j-1)}$, $\mathbf{E}_{\mathrm{B},b}^{(j-1)}$ is updated to $\mathbf{E}_{\mathrm{B},b}^{(j)}$ as

$$\mathbf{E}_{\mathrm{B},b}^{(j)} = \mathbf{E}_{\mathrm{B},b}^{(j-1)} + \mathbf{V}_{\mathrm{T},b}\mathbf{V}_{\mathrm{T},b}^{H}\tilde{\mathbf{E}}_{\mathrm{B},b}^{(j)}. \tag{13}$$

The above process is repeated J times, and the BS finally transmits $\mathbf{X}_b^{(J)} = \mathbf{X}_b + \mathbf{E}_{\mathrm{R},b}^{(J)} + \mathbf{E}_{\mathrm{B},b}^{(J)}$.

In the proposed method, interference component $\mathbf{H}_{\mathrm{T},b}\mathbf{E}_b = \mathbf{H}_{\mathrm{T},b}(\mathbf{E}_{\mathrm{R},b}^{(J)} + \mathbf{E}_{\mathrm{B},b}^{(J)})$ due to the PAPR reduction signal in $\mathbf{Y}_{\mathrm{U},b}$ in (4) is zero in principle. Therefore, the proposed method reduces the PAPR at the RS transmitter in addition to that at the BS transmitter by only using the signal processing at the BS, while suppressing the interference to the data stream at the UE receivers.

The potential limitations of the proposed method are that it cannot address the PAPR at the RS caused by noise added on the RS receiver end and that it incurs a large calculation cost per iteration. However, Fig. 3 in Section IV shows that the proposed method reduces the PAPR at the RS with almost no problem. Fig. 10 shows that the proposed method increases the throughput for the same number of real multiplications compared to the CF for the BS.

IV. NUMERICAL RESULTS

A. SIMULATION PARAMETERS

The performance of the proposed method is evaluated based on computer simulations. Table 1 gives the major simulation parameters. The number of BS transmitter antennas, N_{B}, is set to 100. The number of RS antennas, N_{R}, is 50. The number of UEs, N_{U}, is four. The number of OFDM signal subcarriers, K, is set to 512 and the number of frequency blocks, B, is parameterized. The number of FFT/IFFT points, F, is set to 2048, which corresponds to four-times over-sampling in the time domain in order to measure the PAPR levels accurately [34]. For evaluation generality, we assume that the symbol constellation of each subcarrier follows an independent standard complex Gaussian distribution. ZF-based BF is applied. As the channel model, we assume block Rayleigh fading, which is independent between any pairs of transmitter and receiver antennas and between any frequency blocks. D_{BR} and D_{RU} are fixed to 1 and D_{BU} is parameterized. For propagation distance D, the distance-dependent path loss is set to $1/D^4$.

The power threshold, T, in the clipping process in CF for generating PAPR reduction signals is defined as

$$T = 10\log_{10}\left(\frac{|A_{\max}|^2}{P_{\mathrm{total}}/FN_{\mathrm{t}}}\right)\mathrm{dB} \tag{14}$$

where $A_{\max}$ is the maximum allowable amplitude for clipping the signal, P_{total} is the total transmission power, and N_{t} is the number of transmission antennas. The power thresholds in the CF process for generating PAPR reduction signals for the BS and RS transmitters are denoted as T_{B} and T_{R}, respectively. The number of iterations of the PAPR reduction process, J, is mainly set to 20, since the PAPR reduction gain of the proposed method is almost unchanged after approximately the 20th iteration (refer to Fig. 4).

We evaluate the PAs at the BS and RS assuming linear PAs (IV-C) and non-linear PAs (IV-D), respectively.

In Section IV-C, A_{B} and A_{R} are 1, and $\mathbf{D}_{\mathrm{B},b}$ and $\mathbf{D}_{\mathrm{R},b}$ are zero. The transmission signal at the BS transmitter after PAPR reduction is scaled so that the total transmission power is maintained at a constant value $P_{\mathrm{B,total}}$. The signal-to-noise ratio (SNR) between the BS and RS is defined as

$$\mathrm{SNR} = 10\log_{10}\left(\frac{P_{\mathrm{B,\,total}}}{\sum_{b=1}^{B}\sum_{n=1}^{N_{\mathrm{R}}}\left\|\mathbf{z}_{\mathrm{R},b,n}\right\|^2}\right)\mathrm{dB} \tag{15}$$

where $\mathbf{z}_{\mathrm{R},b,n}$ is the K/B-dimensional noise vector observed at the RS receiver antenna n in frequency block b. The SNR between the RS and UEs is defined as

$$\mathrm{SNR} = 10\log_{10}\left(\frac{P_{\mathrm{B,\,total}}}{\sum_{b=1}^{B}\sum_{n=1}^{N_{\mathrm{U}}}\left\|\mathbf{z}_{\mathrm{U},b,n}\right\|^2}\right)\mathrm{dB} \tag{16}$$

where $\mathbf{z}_{\mathrm{U},b,n}$ is the K/B-dimensional noise vector observed at the UE n in frequency block b. Both SNRs are set to 15 dB.

In Section IV-D, the non-linear PAs at the BS and RS are simulated using the solid state power amplifier (SSPA) model [35] where

$$y(t) = G_0\frac{x(t)}{(1+(|x(t)|/A_{\mathrm{SAT}})^{2p})^{1/2p}}. \tag{17}$$

In (17), the input and the output signals are respectively denoted as $x(t)$ and $y(t)$ at time t. G_0 is the amplification gain in the linear domain of the amplifier and A_{SAT} is the saturation value of the input amplitude. p is the parameter controlling the smoothness of the transition from the linear region to the saturation region. The IBO is defined as

$$\mathrm{IBO} = 10\log_{10}\left(\frac{A_{\mathrm{SAT}}^2}{P_{\mathrm{total}}/FN_{\mathrm{t}}}\right)\mathrm{dB}. \tag{18}$$

The IBOs of the PA at the BS and RS are denoted as $\mathrm{IBO}_{\mathrm{B}}$ and $\mathrm{IBO}_{\mathrm{R}}$, respectively. When the transmission signal is input in the non-linear region, interference signals are added in and out of the band. In this evaluation, G_0 is set to 1, A_{SAT} is 0.05, and p is set to 2.0 referring to [36]. The SNR between the BS and RS is defined as

$$\mathrm{SNR} = 10\log_{10}\left(\frac{A_{\mathrm{SAT}}^2 N_{\mathrm{B}}F}{\sum_{b=1}^{B}\sum_{n=1}^{N_{\mathrm{R}}}\left\|\mathbf{z}_{\mathrm{R},b,n}\right\|^2}\right)\mathrm{dB} \tag{19}$$

TABLE 1. Simulation parameters.

Number of BS antennas, N_{B}	100
Number of RS antennas, N_{R}	50
Number of UEs, N_{U}	4
Number of subcarriers, K	512
Number of frequency blocks, B	Parameterized
Number of FFT/IFFT points, F	2048
Constellation of data modulation	i.i.d. complex Gaussian distributed
BF	Zero-forcing
Channel model	Block Rayleigh No fading correlations between any pair of transmitter and receiver antennas and between any pair of frequency blocks
Distance-dependent path loss	$1/D^4$
Distance between BS and RS, D_{BR}	1
Distance between RS and UE, D_{RU}	1
Distance between BS and UE, D_{BU}	Parameterized
Channel coding	Ideal channel coding
Throughput calculation	Shannon formula where the Bussgang theorem is taken into account

and set to 15 dB. The SNR between the RS and UEs is defined as

$$\mathrm{SNR} = 10\log_{10}\left(\frac{A_{\mathrm{SAT}}^2 N_{\mathrm{R}} F}{\sum_{b=1}^{B}\sum_{n=1}^{N_{\mathrm{U}}}\left\|\mathbf{z}_{\mathrm{U},b,n}\right\|^2}\right)\mathrm{dB} \tag{20}$$

and set to 12 dB. We mainly evaluate the throughput when the required adjacent channel leakage ratio (ACLR) is satisfied. T_{B}, T_{R}, $\mathrm{IBO}_{\mathrm{B}}$, and $\mathrm{IBO}_{\mathrm{R}}$ for each method are set to a combination where the ACLR is larger than the required value and the throughput is as high as possible to make a fair comparison. The definition of ACLR is given in Section IV-*B*.

B. DEFINITIONS OF PAPR, THROUGHPUT, AND ACLR

The PAPR is defined as the ratio of the peak signal power to the average signal power across all the transmitter antennas per OFDM symbol and is represented as

$$\mathrm{PAPR} = 10\log_{10}\left(\frac{\max_{n,t}|x_n(t)|^2}{P_{\mathrm{total}}/FN_{\mathrm{t}}}\right)\mathrm{dB} \tag{21}$$

where $x_n(t)$ represents the time domain transmission signal at time t at antenna n. The performance of any PAPR reduction technique is normally described using the complementary cumulative distribution function (CCDF) diagram. The CCDF of the PAPR is defined as the probability that the PAPR exceeds given threshold value PAPR_0 given by

$$\mathrm{CCDF} = 1 - \Pr\{\mathrm{PAPR} \le \mathrm{PAPR}_0\}. \tag{22}$$

Hereafter, in frequency block b, the K/B-dimensional data stream vector before BF at stream n and the K/B-dimensional received signal vector at UE n are denoted as $\mathbf{s}_{b,n}$ and $\mathbf{y}_{\mathrm{U},b,n}$, respectively. Defining $\tilde{\mathbf{y}}_{\mathrm{U},b,n}$ and $\mathbf{w}_{b,n}$ as the data signal component vector and the interference and noise signal component vector in $\mathbf{y}_{\mathrm{U},b,k}$, respectively, (6) can be expressed as

$$\begin{aligned}\mathbf{Y}_{\mathrm{U},b} &= \left[\mathbf{y}_{\mathrm{U},b,1}\cdots\mathbf{y}_{\mathrm{U},b,N_{\mathrm{U}}}\right]^T \\ &= A_{\mathrm{B}}\left[\mathbf{s}_{b,1}\cdots\mathbf{s}_{b,N_{\mathrm{U}}}\right]^T + \left[\mathbf{w}_{b,1}\cdots\mathbf{w}_{b,N_{\mathrm{U}}}\right]^T \\ &= \left[\tilde{\mathbf{y}}_{\mathrm{U},b,1}\cdots\tilde{\mathbf{y}}_{\mathrm{U},b,N_{\mathrm{U}}}\right]^T + \left[\mathbf{w}_{b,1}\cdots\mathbf{w}_{b,N_{\mathrm{U}}}\right]^T\end{aligned} \tag{23}$$

where $\tilde{\mathbf{y}}_{\mathrm{U},b,n} = A_{\mathrm{B}}\mathbf{s}_{b,n}$ holds. As shown in [37], based on Bussgang's theorem, $\mathbf{w}_{b,n}$ can be written as $\mathbf{w}_{b,n} = (\alpha_{b,n} - 1)\tilde{\mathbf{y}}_{\mathrm{U},b,n} + \mathbf{d}_{b,n}$, where

$$\alpha_{b,n} = \frac{\tilde{\mathbf{y}}_{\mathrm{U},b,n}^H \mathbf{y}_{\mathrm{U},b,n}}{\left\|\tilde{\mathbf{y}}_{\mathrm{U},b,n}\right\|^2} \tag{24}$$

and $\mathbf{d}_{b,n}$ is uncorrelated with $\tilde{\mathbf{y}}_{\mathrm{U},b,n}$. The sum throughput of N_{U} streams (users) is calculated based on the Shannon formula, which corresponds to the upper limit of the transmission rate that can be transmitted without error using ideal channel coding. The sum throughput is.

$$C = \frac{1}{B}\sum_{b=1}^{B}\sum_{n=1}^{N_{\mathrm{U}}}\log_2\left(1 + \frac{\left\|\alpha_{b,n}\tilde{\mathbf{y}}_{\mathrm{U},b,n}\right\|^2}{\left\|\mathbf{d}_{b,n}\right\|^2}\right) \tag{25}$$

In ACLR measurements, the assigned channel bandwidth, W, including the guard band is defined as $W = (10/9)K$ in terms of the number of subcarriers, referring to 5G NR specifications with a bandwidth of 5 MHz and subcarrier spacing of 15 kHz [38]. In this simulation, W corresponds to approximately 570 subcarriers. The center frequency of the adjacent channel is defined as W away from the center frequency of the assigned channel. The ACLR is defined as

$$\mathrm{ACLR} = 10\log_{10}\frac{P_{\mathrm{C}}}{P_{\mathrm{U}}}\mathrm{dB} \tag{26}$$

where P_{C} and P_{U} are the average power in the band equivalent to K subcarriers of the assigned channel and the adjacent channel, respectively. Note that in 5G NR, the ACLR requirement is 45 dB or higher for a BS operating in bands other than band n46, n96, n102, and n104 [38].

C. SIMULATION RESULTS USING LINEAR PA

Fig. 3 shows the CCDF of the PAPR at the BS and RS. For comparison, the method that reduces only the PAPR at the BS transmitter utilizing the null space of the channel (henceforth referred to as null space-based PAPR reduction for the BS), the CF for the BS [27], and no PAPR reduction at the BS and RS are shown in addition to the proposed method. Both T_{B} and T_{R} in the proposed method are set to 3 dB. T_{B} in the null space-based PAPR reduction for the BS and the CF for the BS is set to 3 dB. J is set to 20, D_{BU} is set to 2 and B is set to 8. The figure shows that the PAPR levels at the BS and RS are simultaneously reduced using the proposed method. This is because the proposed method generates and transmits a PAPR reduction signal from the BS, which reduces the PAPR at the BS and RS. On the other hand, in the null space-based PAPR reduction for the BS and the CF for the BS, the PAPR level at the BS can be reduced, but the PAPR level at the

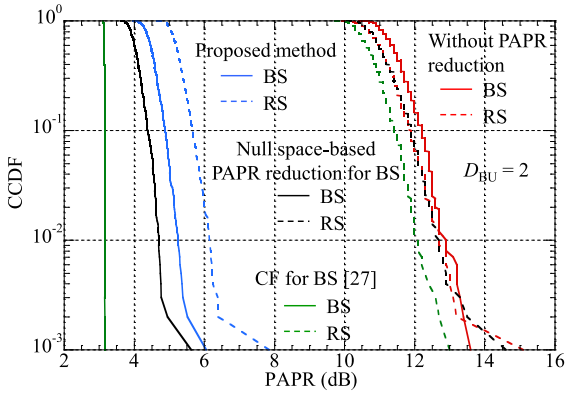

FIGURE 3. CCDF of PAPR at BS and RS.

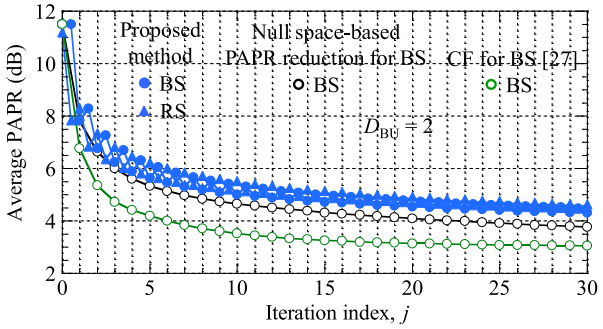

FIGURE 4. Average PAPR at BS and RS as a function of iteration index.

RS is almost the same as those without PAPR reduction for both the BS and RS. This is because, in the MIMO relay transmission, the received signal at the RS is a superposition of many transmission signals from the BS.

Fig. 4 shows the average PAPR at the BS and RS as a function of iteration index j. For comparison, the PAPR levels at the BS in the null space-based PAPR reduction for the BS and the CF for the BS are shown in addition to the PAPR levels at the BS and RS for the proposed method. As described in Section III, the proposed method performs the PAPR reduction process for the BS transmission signal after the PAPR reduction process for the RS transmission signal at each iteration. In Fig. 4, the PAPR at the j-th iteration represents the PAPR level after the PAPR reduction process for the BS transmission signal. The PAPR level shown between the j-th and j+1-th iterations in the proposed method represents the PAPR level after the PAPR reduction process for the RS transmission signal. Both T_B and T_R in the proposed method are set to 3 dB. T_B in the null space-based PAPR reduction for the BS and the CF for the BS is set to 3 dB. D_{BU} is set to 2 and B is set to 8. In the proposed method, after the PAPR reduction process for the RS transmission signal, the PAPR at the RS decreases, but the PAPR at the BS increases. On the other hand, after the PAPR reduction process for the BS transmission signal, the PAPR at the BS decreases, but the PAPR at the RS increases. This is because the signal that decreases the PAPR at the RS increases the PAPR at the BS and vice versa. However, as the number of iterations increases, the oscillations caused by increasing and decreasing the PAPR become smaller and the overall PAPR levels at the BS and RS decrease. This is because a more accurate PAPR reduction signal is generated for both the BS and RS as the process is iterated considering the existence of the PAPR signal for another node (the RS for the BS and the BS for the RS). However, the oscillation of the PAPR at the BS in the proposed method converges at a higher level PAPR at the BS than that for the null space-based PAPR reduction for the BS, assuming the same T_B of 3 dB. The CF for the BS is the most effective for PAPR reduction because it does not project the PAPR reduction signal onto the null space of the channel.

Fig. 5 shows the average throughput as a function of the average PAPR at the BS and RS with the number of frequency blocks B as a parameter. For comparison, the null space-based PAPR reduction for the BS and the CF for the BS are shown in addition to the proposed method. T_B and T_R in the proposed method are set to equal values, and by changing these values in each method, the relationship between the average PAPR at the RS and the average throughput is varied. J is set to 20, D_{BU} is set to 2. As the number of frequency blocks, B, increases, the PAPR at the BS and RS decreases and the throughput increases in all methods. This is because the PAPR reduction signal component appearing in the null space of the channel is expected to increase as the frequency selectivity of the channel increases. The proposed method achieves a better average PAPR at the BS as a function of the average throughput than that for the CF for the BS. This is because the interference caused by the PAPR reduction signal observed at the UE, which occurs when CF is used at the BS, is reduced by projecting the PAPR reduction signal onto the null space of the channel in the proposed method. When comparing the performance at the BS for the proposed method to that for the null space-based PAPR reduction for the BS, the proposed method appears to be worse. This is because the proposed method reduces the data signal power transmitted by the BS due to the BS transmitting a PAPR reduction signal for the RS in addition to the PAPR reduction signal for the BS. This reduces the throughput and increases the PAPR at the BS due to the PAPR reduction process for the RS.

D. SIMULATION RESULTS USING NON-LINEAR PA

Fig. 6 shows the transmission signal spectrum at the BS and RS. The required ACLR is set to 45 dB for the BS and RS. J is set to 20, D_{BU} is set to 2 and B is set to 8. In addition to the proposed method, the characteristics when there is no PAPR reduction at the BS and RS are shown. T_B, T_R, and IBO for each method are shown in the figure. The signal power normalized by the average power per subcarrier, P_C/K, in the band of the assigned channel is represented on the vertical axis. The frequency normalized by the assigned channel bandwidth, W, including the guard band is represented on the horizontal axis. The transmission spectrum at the BS in the proposed method is more nicely shaped than that in

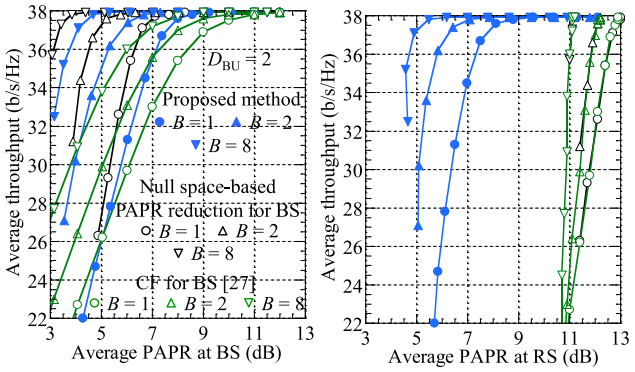

FIGURE 5. Average throughput as a function of average PAPR at BS and RS with the number of frequency blocks as a parameter.

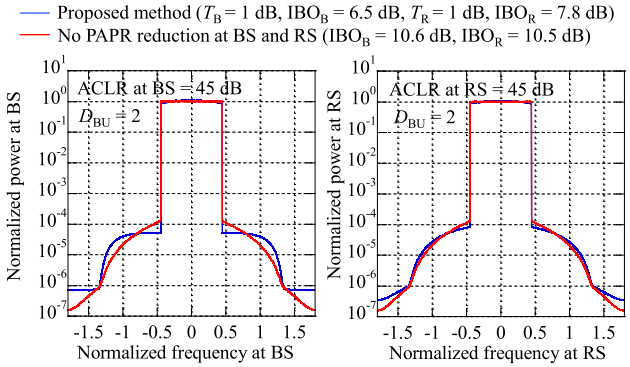

FIGURE 6. Transmission signal spectrum at BS and RS.

the method without PAPR reduction. On the other hand, the transmission spectrum at the RS in the proposed method is more similar to that for the method without PAPR reduction. This is because although the proposed method reduces the PAPR at the RS through signal processing at the BS, it does not address the PAPR at the RS caused by non-linearity in the PA at the BS and noise added on the RS receiver end.

Fig. 7 shows the average throughput, IBO$_B$, and IBO$_R$ as a function of the number of frequency blocks, B. The required ACLR is set to 45 dB for the BS and RS. J is set to 20, D_{BU}, is set to 2. In addition to the proposed method, the null space-based PAPR reduction for the BS and the CF for the BS are tested for comparison. Regardless of the PAPR reduction method, as the number of frequency blocks, B, increases, in other words, as the frequency selectivity of the channel increases, the throughput increases and the IBO in the non-linear amplifier decreases. This is because the increase in the frequency selectivity of the channel increases the PAPR reduction signal component appearing in the null space of the channel. The proposed method and the null space-based PAPR reduction for the BS increase the throughput compared to that for the CF for the BS. This is because the proposed method and the null space-based PAPR reduction for the BS can reduce the IBO$_B$ to less than that for the CF for the BS by utilizing the null space of the channel to suppress interference to the data stream caused by the PAPR reduction signal. However, as the frequency selectivity of the channel increases, the PAPR reduction signal component appearing in the null space of the channel increases in the CF for the BS as well. Thus, the IBO$_B$ level in the CF for the BS becomes close to that in the proposed method and the null space-based PAPR reduction for the BS. The proposed method increases the throughput compared to the null space-based PAPR reduction for the BS. This is because the proposed method reduces the PAPR at the RS through signal processing at the BS. As a result, the proposed method reduces the IBO$_R$ compared to the null space-based PAPR reduction for the BS. The IBO$_B$ of the proposed method is slightly larger than that for the null space-based PAPR reduction for the BS. This is because, as discussed in relation to Fig. 4, in the proposed method, the signal that reduces the PAPR at the RS causes an increase in the PAPR at the BS.

Fig. 8 shows the average throughput, IBO$_B$, and IBO$_R$ as a function of the required ACLR at the RS. The required ACLR at the BS is set to 45 dB. J is set to 20, D_{BU} is set to 2 and B is set to 8. In addition to the proposed method, the null space-based PAPR reduction for the BS and the CF for the BS are tested for comparison. The throughput decreases as the required ACLR for the RS increases. This is because the IBO$_R$ increases to achieve the required ACLR value, resulting in a lower effective SNR. Regardless of the required ACLR at the RS, the proposed method achieves a higher throughput than the other methods. This is because the proposed method performs PAPR reduction not only for the BS but also for the RS through signal processing at the BS, while utilizing the null space of the channel. Based on the above, it can be said that it is important to reduce the PAPR at the RS regardless of the required ACLR at the RS to achieve a higher throughput.

Fig. 9 shows the average throughput, IBO$_B$, and IBO$_R$ as a function of D_{BU}. The required ACLR at the BS and RS is set to 45 dB. J is set to 20 and B is set to 8. In addition to the proposed method, the null space-based PAPR reduction for the BS and the CF for the BS are tested for comparison. Overall, the throughput levels of all methods are increased as D_{BU} decreases thanks to the increased direct link gain. The proposed method achieves a higher throughput than the other methods regardless of D_{BU}. This is because the proposed method performs PAPR reduction not only for the BS but also for the RS through signal processing at the BS, while utilizing the null space of the channel. The throughput level of the null space-based PAPR reduction for the BS is close to that for the proposed method as the D_{BU} decreases. This is because the received signal power from the direct link increases relative to that from the relay link as the D_{BU} decreases, and thus IBO$_R$ has a smaller impact on the effective SNR. On the other hand, the throughput level of the null space-based PAPR reduction for the BS is close to that for the CF for the BS as D_{BU} increases. This is because the received signal power from the direct link decreases relative to that from the relay link as D_{BU} increases, and therefore the high IBO$_R$ has a greater impact on the effective SNR. Since the proposed method reduces the

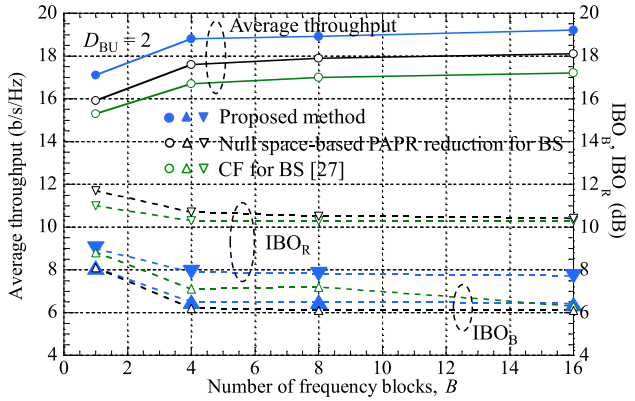

FIGURE 7. Average throughput, IBO_B, and IBO_R as a function of the number of frequency blocks, B.

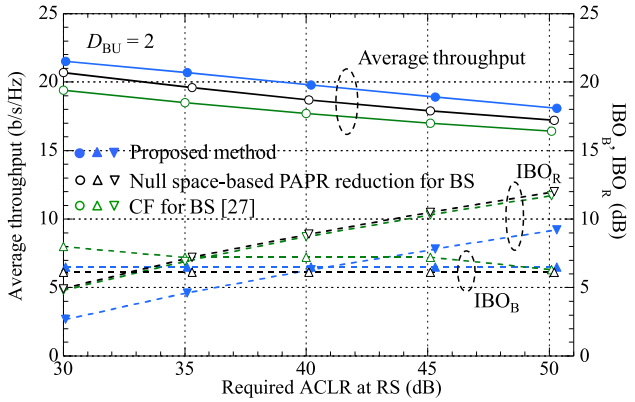

FIGURE 8. Average throughput, IBO_B, and IBO_R as a function of required ACLR at RS.

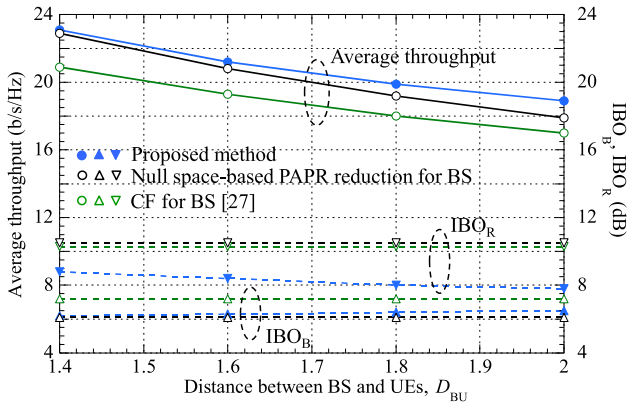

FIGURE 9. Average throughput, IBO_B, and IBO_R as a function of distance between BS and UEs, D_{BU}.

IBO_R, the throughput level of the proposed method can have a constant gain over the CF for the BS even if D_{BU} increases.

The required calculation cost per iteration depends on the PAPR reduction method. In the following, we compare the throughput of each method for the same computational complexity. In this paper, we use the required number of real multiplications for each method to evaluate the computational complexity. Table 2 gives the number of real multiplications per iteration for each PAPR reduction method.

TABLE 2. Number of real multiplications for each PAPR reduction method.

PAPR Reduction Method	Process	Number of Real Multiplications
Proposed method	Generation of Moore-Penrose inverse of channel matrix between BS and RS	$4N_R^2(N_R+2N_B)B$
	Calculation of null space matrix and Moore-Penrose inverse	$4N_B^2(N_B+N_R-N_U)$
	Prediction of received signal at RS	$4JN_BFN_R$
	IFFT	$4J(N_B+N_R)F\log_2 F$
	Power measurement of transmission signal	$2J(N_B+N_R)F$
	Amplitude clipping	$3J(N_B+N_R)F$
	FFT	$4J(N_B+N_R)F\log_2 F$
	Projection onto null space	$4JN_BF(N_B+N_R)$
Null space-based PAPR reduction for BS	Calculation of null space matrix	$4N_B^2(N_B-N_U)$
	IFFT	$4JN_BF\log_2 F$
	Power measurement of transmission signal	$2JN_BF$
	Amplitude clipping	$3JN_BF$
	FFT	$4JN_BF\log_2 F$
	Projection onto null space	$4JN_B^2F$
CF for BS [27]	IFFT	$4JN_BF\log_2 F$
	Power measurement of transmission signal	$2JN_BF$
	Amplitude clipping	$3JN_BF$
	FFT	$4JN_BF\log_2 F$

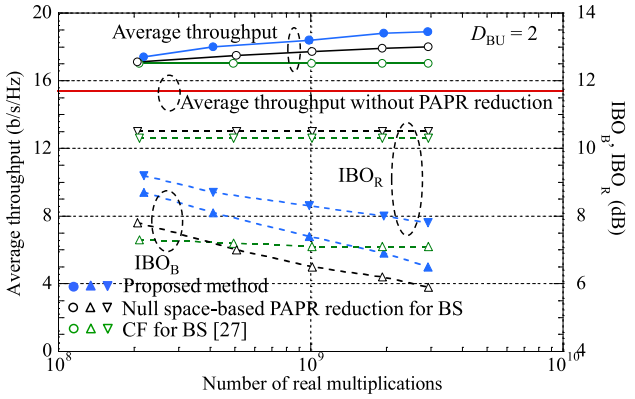

FIGURE 10. Average throughput, IBO_B, and IBO_R as a function of the number of real multiplications.

Based on Table 2, Fig. 10 shows the throughput as a function of the number of real multiplications. The required ACLR at the BS and RS is set to 45 dB. B is set to 8. In addition to the proposed method, the null space-based PAPR reduction for the BS and the CF for the BS are tested for comparison. The average throughput without PAPR reduction is also shown to confirm that a higher throughput can be achieved with PAPR reduction. Without PAPR reduction at the BS and RS, the throughput is significantly degraded due to large IBO_B and IBO_R values (The IBO_B and IBO_R levels are shown in Fig. 6). Although the proposed method requires more real multiplications per iteration, it achieves the highest throughput compared to other methods with the same number of real multiplications. This is because the proposed method reduces the PAPR at the BS and RS and can reduce the IBO_R as well as the IBO_B. The throughput levels for the proposed method and the null space-based PAPR reduction for the BS are increased as the number of real multiplications of the PAPR reduction signal processing is increased. This is because as the number of iterations of the PAPR reduction process increases, the PAPR is sufficiently reduced to make the IBO smaller. On the other hand, the throughput level of

the CF for the BS barely increases as the number of real multiplications of the PAPR reduction signal processing is increased. This is because the CF for the BS requires fewer real number multiplications per iteration, so it can perform more iterations than the method utilizing the null space of the channel when compared with the same number of real multiplications, and the PAPR reduction effect per iteration is great. However, since the CF for the BS causes interference to the data stream at the UE receiver, increasing the number of iterations does not improve the throughput much. In the null space-based PAPR reduction for the BS, increasing the number of iterations of the PAPR reduction process does little to improve the throughput. This is because there is a limit to the improvement in the throughput simply by reducing the PAPR at the BS. The proposed method improves the throughput gain more than does the null space-based PAPR reduction for the BS when the number of real multiplications is increased. This is because the proposed method reduces the PAPR at the RS as well as at the BS through signal processing at the BS. The above results show that it is important to reduce the PAPR not only at the BS but also at the RS and to suppress interference to the data stream due to the PAPR reduction signal to achieve higher throughput by increasing the number of iterations of the PAPR reduction process.

V. CONCLUSION

We proposed a novel PAPR reduction method utilizing the null space in the overall channel of the entire system with frequency selectivity for the RS transmitter by relying only on the signal processing at the BS in downlink MIMO-OFDM transmission using AF-type relaying. The proposed method alternately and repeatedly generates signals to reduce the PAPR at the BS and signals to reduce the PAPR at the RS through signal processing at the BS. The generated signals are projected onto the null space of the overall channel of the entire system at each frequency block and the resultant PAPR reduction signals are transmitted from the BS. The proposed method achieves PAPR reduction both for the BS and RS without any PAPR reduction signal processing with a transmission delay at the RS while suppressing interference to the data stream caused by the PAPR reduction signals. Computer simulation results using the SSPA model show that reducing the PAPR not only at the BS but also at the RS is effective in achieving a higher throughput. The proposed method achieves a higher throughput than that for the other methods regardless of the number of frequency blocks, the required ACLR at the RS, and the distance between the BS and UE.

In the future, we plan to reduce the calculation cost of the BS in the proposed method. Furthermore, channel estimation errors may degrade the accuracy of the PAPR reduction for the RS transmitter, projection of the PAPR reduction signal onto the null space of the channel, and the accuracy of BF based on ZF. Therefore, we also plan to take into account the channel estimation error in further studies on the proposed method.

REFERENCES

[1] T. L. Marzetta, "Noncooperative cellular wireless with unlimited numbers of base station antennas," *IEEE Trans. Wireless Commun.*, vol. 9, no. 11, pp. 3590–3600, Nov. 2010.

[2] H. Papadopoulos, C. Wang, O. Bursalioglu, X. Hou, and Y. Kishiyama, "Massive MIMO technologies and challenges towards 5G," *IEICE Trans. Commun.*, vol. E99-B, no. 3, pp. 602–621, Mar. 2016.

[3] E. Dahlman, S. Parkvall, and J. Skold, *5G NR: The Next Generation Wireless Access Technology*. New York, NY, USA: Academic, 2018.

[4] *White Paper: 5G Evolution and 6G*, NTT DOCOMO, Jan. 2022.

[5] R. U. Nabar, H. Bolcskei, and F. W. Kneubuhler, "Fading relay channels: Performance limits and space–time signal design," *IEEE J. Sel. Areas Commun.*, vol. 22, no. 6, pp. 1099–1109, Aug. 2004.

[6] H. Bolcskei, R. U. Nabar, O. Oyman, and A. J. Paulraj, "Capacity scaling laws in MIMO relay networks," *IEEE Trans. Wireless Commun.*, vol. 5, no. 6, pp. 1433–1444, Jun. 2006.

[7] K. Tateishi and K. Higuchi, "Adaptive amplify-and-forward relaying for cellular downlink," *IEICE Trans. Commun.*, vol. E96-B, no. 7, pp. 1968–1975, Jul. 2013.

[8] S. H. Han and J. H. Lee, "An overview of peak-to-average power ratio reduction techniques for multicarrier transmission," *IEEE Wireless Commun.*, vol. 12, no. 2, pp. 56–65, Apr. 2005.

[9] X. Li and L. J. Cimini Jr., "Effect of clipping and filtering on the performance of OFDM," *IEEE Commun. Lett.*, vol. 2, no. 5, pp. 131–133, May 1998.

[10] J. Armstrong, "Peak-to-average power reduction for OFDM by repeated clipping and frequency domain filtering," *Electron. Lett.*, vol. 38, no. 5, pp. 246–247, Feb. 2002.

[11] B. S. Krongold and D. L. Jones, "PAR reduction in OFDM via active constellation extension," *IEEE Trans. Broadcast.*, vol. 49, no. 3, pp. 258–268, Sep. 2003.

[12] A. Aggarwal and T. H. Meng, "Minimizing the peak-to-average power ratio of OFDM signals using convex optimization," *IEEE Trans. Signal Process.*, vol. 54, no. 8, pp. 3099–3110, Aug. 2006.

[13] J. Tellado and J. M. Cioffi, "Efficient algorithms for reducing PAR in multicarrier systems," in *Proc. IEEE Int. Symp. Inf. Theory*, Cambridge, MA, USA, Aug. 1998, p. 191.

[14] H. Lee, D. N. Liu, W. Zhu, and M. P. Fitz, "Peak power reduction using a unitary rotation in multiple transmit antennas," in *Proc. IEEE Int. Conf. Commun.*, Seoul, South Korea, May 2005, pp. 2407–2411.

[15] G. R. Woo and D. L. Jones, "Peak power reduction in MIMO OFDM via active channel extension," in *Proc. IEEE Int. Conf. Commun.*, Seoul, South Korea, May 2005, pp. 2636–2639.

[16] S. Suyama, H. Adachi, H. Suzuki, and K. Fukawa, "PAPR reduction methods for eigenmode MIMO-OFDM transmission," in *Proc. IEEE 69th Veh. Technol. Conf.*, Barcelona, Spain, Apr. 2009, pp. 1–5.

[17] H. Ando and K. Higuchi, "Comparison of PAPR reduction methods for OFDM signal with channel coding," in *Proc. APWCS*, Seoul, South Korea, Aug. 2009.

[18] H. Prabhu, O. Edfors, J. Rodrigues, L. Liu, and F. Rusek, "A low-complex peak-to-average power reduction scheme for OFDM based massive MIMO systems," in *Proc. 6th Int. Symp. Commun., Control Signal Process. (ISCCSP)*, Athens, Greece, May 2014, pp. 114–117.

[19] T. Kageyama, O. Muta, and H. Gacanin, "Enhanced peak cancellation with simplified in-band distortion compensation for massive MIMO-OFDM," *IEEE Access*, vol. 8, pp. 73420–73431, 2020.

[20] Y. Sato, M. Iwasaki, S. Inoue, and K. Higuchi, "Clipping and filtering-based adaptive PAPR reduction method for precoded OFDM-MIMO signals," *IEICE Trans. Commun.*, vol. E96-B, no. 9, pp. 2270–2280, Sep. 2013.

[21] S. Inoue, T. Kawamura, and K. Higuchi, "Throughput/ACLR performance of CF-based adaptive PAPR reduction method for eigenmode MIMO-OFDM signals with AMC," in *Proc. IEICE Trans. Commun.*, vol. E96-B, no. 9, pp. 2293–2300, Sep. 2013.

[22] R. Kimura, Y. Tajika, and K. Higuchi, "CF-based adaptive PAPR reduction method for block diagonalization-based multiuser MIMO-OFDM signals," in *Proc. IEEE 73rd Veh. Technol. Conf.*, Budapest, Hungary, May 2011, pp. 1–5.

[23] T. Suzuki, M. Suzuki, Y. Kishiyama, and K. Higuchi, "Complexity-reduced adaptive PAPR reduction method using null space in MIMO channel for MIMO-OFDM signals," *IEICE Trans. Commun.*, vol. E103-B, no. 9, pp. 1019–1029, Sep. 2020.

[24] T. Suzuki, M. Suzuki, and K. Higuchi, "Parallel peak cancellation signal-based PAPR reduction method using null space in MIMO channel for MIMO-OFDM transmission," *IEICE Trans. Commun.*, vol. E104-B, no. 5, pp. 539–549, May 2021.
[25] R. Zayani, H. Shaiek, and D. Roviras, "PAPR-aware massive MIMO-OFDM downlink," *IEEE Access*, vol. 7, pp. 25474–25484, 2019.
[26] L. Hua, Y. Wang, Z. Lian, Y. Su, and Z. Xie, "Low-complexity PAPR-aware precoding for massive MIMO-OFDM downlink systems," *IEEE Wireless Commun. Lett.*, vol. 11, no. 7, pp. 1339–1343, Jul. 2022.
[27] M. Eddaghel and J. A. Chambers, "PAPR reduction in distributed amplify-and-forward type closed loop extended orthogonal space frequency block coding with one-bit group feedback for cooperative communications," in *Proc. 18th Eur. Wireless Conf.*, Poznan, Poland, 2012, pp. 1–6.
[28] S. Yang, W. Yang, Y. Cai, and W. Li, "An energy efficient PTS scheme for PAPR reduction in OFDM relay systems," in *Proc. 10th Int. Conf. Commun. Netw. China (ChinaCom)*, Shanghai, China, Aug. 2015, pp. 858–863.
[29] G. Bai, Z. Zhong, R. Xu, G. Wang, and Z. Qin, "Golay complementary sequences and Reed–Müller codes based PAPR reduction for relay networks with superimposed training," in *Proc. IEEE 11th Int. Conf. Signal Process.*, vol. 2. Beijing, China, Oct. 2012, pp. 1558–1561.
[30] N. B. Harum, K. Yuda, and T. Ohtsuki, "PAPR reduction of amplify-and-forward relay OFDM system using subcarrier pairing method," in *Proc. IEEE 24th Annu. Int. Symp. Pers., Indoor, Mobile Radio Commun. (PIMRC)*, Sep. 2013, pp. 2005–2010.
[31] Y. Sekiguchi, N. Nonaka, and K. Higuchi, "PAPR reduction using null space in MIMO channel for MIMO-OFDM signals in multiple-antenna AF relay transmission," in *Proc. IEEE 94th Veh. Technol. Conf.*, Sep. 2021, pp. 1–5.
[32] Y. Sekiguchi, N. Nonaka, and K. Higuchi, "PAPR reduction of OFDM signals using null space in MIMO channel for MIMO amplify-and-forward relay transmission," *IEICE Trans. Commun.*, vol. E105-B, no. 9, pp. 1078–1086, Sep. 2022.
[33] A. Kakehashi, N. Nonaka, and K. Higuchi, "PAPR reduction using null space in MIMO channel based on signal processing at base station for downlink AF-based relaying MIMO-OFDM signals," in *Proc. IEEE 96th Veh. Technol. Conf.*, Sep. 2022, pp. 1–6.
[34] M. Sharif, M. Gharavi-Alkhansari, and B. H. Khalaj, "On the peak-to-average power of OFDM signals based on oversampling," *IEEE Trans. Commun.*, vol. 51, no. 1, pp. 72–78, Jan. 2003.
[35] C. Dudak, A. T. Koc, and S. Koc, "Solid state power amplifier (SSPA) non-linearity effects on quadri-phase shift keying modulation," in *Proc. EuWiT*, Amsterdam, Netherlands, Oct. 2004, pp. 237–240.
[36] E. Costa and S. Pupolin, "M-QAM-OFDM system performance in the presence of a nonlinear amplifier and phase noise," *IEEE Trans. Commun.*, vol. 50, no. 3, pp. 462–472, Mar. 2002.
[37] H. Ochiai and H. Imai, "Performance analysis of deliberately clipped OFDM signals," *IEEE Trans. Commun.*, vol. 50, no. 1, pp. 89–101, Jan. 2002.
[38] *NR Base Station (BS) Radio Transmission and Reception (Release 17)*, document TS38.104, 3GPP, 2017.

ASUKA KAKEHASHI (Graduate Student Member, IEEE) received the B.E. degree from the Tokyo University of Science, Noda, Japan, in 2022, where he is currently pursuing the M.E. degree with the Department of Electrical Engineering. His research interest includes wireless communications. He is a Student Member of the IEICE.

TAKANORI HARA (Member, IEEE) received the B.E., M.E., and Ph.D. degrees in engineering from The University of Electro-Communications, Tokyo, Japan, in 2017, 2019, and 2022, respectively. Since April 2022, he has been with the Department of Electrical Engineering, Tokyo University of Science, Chiba, Japan, where he is currently an Assistant Professor. His current research interests include grant-free access, compressed sensing, and MIMO technologies.

KENICHI HIGUCHI (Senior Member, IEEE) received the B.E. degree from Waseda University, Tokyo, Japan, in 1994, and the Dr.Eng. degree from Tohoku University, Sendai, Japan in 2002. In 1994, he joined NTT Mobile Communications Network Inc. (now, NTT DOCOMO Inc.). While with NTT DOCOMO Inc., he was engaged in the research and standardization of wireless access technologies for wideband DS-CDMA mobile radio, HSPA, LTE, and broadband wireless packet access technologies for systems beyond IMT-2000. In 2007, he joined as a Faculty Member of the Tokyo University of Science, where he is currently a Professor. His current research interests include the areas of wireless technologies and mobile communication systems, including advanced multiple access, such as non-orthogonal multiple access (NOMA), radio resource allocation, inter-cell interference coordination, multiple-antenna transmission techniques, signal processing, such as interference cancellation and turbo equalization, and issues related to heterogeneous networks using small cells. He was a co-recipient of the Best Paper Award of the International Symposium on Wireless Personal Multimedia Communications, in 2004 and 2007, the Best Paper Award from the IEICE, in 2021, a recipient of the Young Researcher's Award from the IEICE, in 2003, the Fifth YRP Award, in 2007, the Prime Minister Invention Prize, in 2010, and the Invention Prize of Commissioner of the Japan Patent Office, in 2015. He is a Senior Member of the IEICE.